



**RCS Predictions From a Method of Moments and a
Finite-Element Code for Several Targets**

**by William A. Spurgeon, Robert B. Bossoli, Nicholas Hirth,
and Kenneth Ferreira**

ARL-TR-5234

July 2010

NOTICES

Disclaimers

The findings in this report are not to be construed as an official Department of the Army position unless so designated by other authorized documents.

Citation of manufacturer's or trade names does not constitute an official endorsement or approval of the use thereof.

Destroy this report when it is no longer needed. Do not return it to the originator.

Army Research Laboratory

Aberdeen Proving Ground, MD 21005-5069

ARL-TR-5234

July 2010

RCS Predictions From a Method of Moments and a Finite-Element Code for Several Targets

**William A. Spurgeon and Robert B. Bossoli,
Weapons and Materials Research Directorate, ARL**

**Nicholas Hirth and Kenneth Ferreira
ANSOFT Corporation**

REPORT DOCUMENTATION PAGE			<i>Form Approved</i> OMB No. 0704-0188		
Public reporting burden for this collection of information is estimated to average 1 hour per response, including the time for reviewing instructions, searching existing data sources, gathering and maintaining the data needed, and completing and reviewing the collection information. Send comments regarding this burden estimate or any other aspect of this collection of information, including suggestions for reducing the burden, to Department of Defense, Washington Headquarters Services, Directorate for Information Operations and Reports (0704-0188), 1215 Jefferson Davis Highway, Suite 1204, Arlington, VA 22202-4302. Respondents should be aware that notwithstanding any other provision of law, no person shall be subject to any penalty for failing to comply with a collection of information if it does not display a currently valid OMB control number. PLEASE DO NOT RETURN YOUR FORM TO THE ABOVE ADDRESS.					
1. REPORT DATE (DD-MM-YYYY) July 2010		2. REPORT TYPE Final		3. DATES COVERED (From - To) February 2009–March 2010	
4. TITLE AND SUBTITLE RCS Predictions From a Method of Moments and a Finite-Element Code for Several Targets			5a. CONTRACT NUMBER		
			5b. GRANT NUMBER		
			5c. PROGRAM ELEMENT NUMBER		
6. AUTHOR(S) William A. Spurgeon, Robert B. Bossoli, Nicholas Hirth *, and Kenneth Ferreira *			5d. PROJECT NUMBER 622105H84		
			5e. TASK NUMBER		
			5f. WORK UNIT NUMBER		
7. PERFORMING ORGANIZATION NAME(S) AND ADDRESS(ES) U.S. Army Research Laboratory ATTN: RDRL-WMM-A Aberdeen Proving Ground, MD 21005-5069			8. PERFORMING ORGANIZATION REPORT NUMBER ARL-TR-5234		
9. SPONSORING/MONITORING AGENCY NAME(S) AND ADDRESS(ES)			10. SPONSOR/MONITOR'S ACRONYM(S)		
			11. SPONSOR/MONITOR'S REPORT NUMBER(S)		
12. DISTRIBUTION/AVAILABILITY STATEMENT Approved for public release; distribution is unlimited.					
13. SUPPLEMENTARY NOTES * ANSOFT Corporation, 25 Burlington Mall Rd., 5 th Floor, Burlington, MA 01803					
14. ABSTRACT This report presents results of radar cross section (RCS) calculations for several interesting targets using a method-of-moments code and a finite-element code. A physical optics code does not handle the mechanisms that contribute to the RCS for the targets and was not an option. These two codes calculate the RCS of an object in very different ways, but the results from the two codes agree very well in regions where the RCS is large enough to matter. The predictions of the codes were also in good agreement with experimental data for one of the targets.					
15. SUBJECT TERMS radar cross section, method of moments, finite element, modeling					
16. SECURITY CLASSIFICATION OF:			17. LIMITATION OF ABSTRACT	18. NUMBER OF PAGES	19a. NAME OF RESPONSIBLE PERSON William A. Spurgeon
a. REPORT Unclassified	b. ABSTRACT Unclassified	c. THIS PAGE Unclassified			UU

Contents

List of Figures	iv
1. Introduction	1
2. Results	2
3. Conclusions	19
Distribution List	20

List of Figures

Figure 1. A metal plate meshed for FE analysis with the near-to-far field box (darker) and the perfectly matched layer box lighter also shown.....	2
Figure 2. The model propeller used in the analyses (left) and a real propeller for a small UAV (right).....	3
Figure 3. The calculated 3-GHz RCS at a 0° elevation angle of the model propeller.	3
Figure 4. The 3-GHz RCS at a 0° elevation angle of the model propeller calculated using HFSS.	4
Figure 5. The 10-GHz RCS at a 0° elevation angle of the metal propeller.	4
Figure 6. The 10-GHz RCS at a 0° elevation angle of the model propeller calculated using HFSS.	5
Figure 7. The 10-GHz RCS at a 0° elevation angle of the dielectric propeller.	5
Figure 8. The test arrangement for 8–18 GHz RCS tests.	6
Figure 9. A diagram of the Ka band test arrangement for VV polarization.	7
Figure 10. A close-up view of the propeller mounted for testing.....	7
Figure 11. The 15-GHz RCS at a 0° elevation angle of the metal propeller.	8
Figure 12. The 15-GHz RCS at a 0° elevation angle of the model propeller calculated using HFSS.....	9
Figure 13. The 15-GHz HH RCS for the plastic propeller.	9
Figure 14. The 15-GHz VV RCS for the plastic propeller.	10
Figure 15. The 34-GHz RCS at a 0° elevation angle of the metal propeller.	10
Figure 16. The calculated RCS of the 100-mil-thick 1- × 2-in plate at 34 GHz.....	11
Figure 17. The calculated RCS of the 50-mil-thick 1- × 2-in plate at 34 GHz.....	12
Figure 18. The calculated RCS of the 10-mil-thick 1- × 2-in plate at 34 GHz.....	12
Figure 19. The calculated RCS of the 5-mil-thick 1- × 2-in plate at 34 GHz.....	13
Figure 20. The trihedron analyzed in this study.	13
Figure 21. The 5-GHz RCS at a 5° elevation angle calculated using a MOM code.....	14
Figure 22. The 5-GHz VV RCS at a 5° elevation angle calculated using the MOM code (dark blue) and HFSS (light blue).....	14
Figure 23. The HH polarized 5-GHz RCS at a 5° elevation angle calculated using HFSS (light-green curve) and the MOM code (dark-green curve). The red curve is the VH RCS calculated using the MOM code.	15
Figure 24. The RCS at a 10° elevation angle calculated using a MOM code and HFSS.	15
Figure 25. The HH RCS for the trihedron at a 10° elevation angle calculated using the MOM code (dark green) and using HFSS with increased accuracy (light green).	16

Figure 26. The 5-GHz RCS at a 15° elevation angle calculated using a MOM code and HFSS.....17

Figure 27. The 5-GHz RCS at a 20° elevation angle calculated using a MOM code and HFSS.....17

Figure 28. The 1-in-diameter, 4-in-long cylinder analyzed.....18

Figure 29. The end-on VV RCS of the cylinder calculated using a MOM code (light blue) and HFSS (dark blue).....18

INTENTIONALLY LEFT BLANK.

1. Introduction

There are a significant number of problems in radar cross section (RCS) simulation that require an exact code for solution. In this report, we compare RCS calculations with two very different types of exact code, a method-of-moments (MOM) code and a finite-element (FE) code. Both types of code are exact in that they contain all of the physics in Maxwell's equations: reflection, diffraction, traveling waves, etc. The MOM code recasts Maxwell's equations for the electromagnetic fields as integral equations for the currents on surfaces that can then be solved using numerical methods. Once the currents have been obtained, it is straightforward to calculate the electromagnetic fields in all of space. This works well for metallic targets since the currents are confined to the outer surfaces, which considerably reduces the regions of space that need to be analyzed. With advanced numerical methods, such as the multilayer fast multipole algorithm, the solution time can be acceptably fast.¹ Commercial codes are available.^{2,3} In contrast, the FE method solves Maxwell's equations directly. This requires building a three-dimensional (3-D) grid that includes the target. In order to keep the size of the problem as small as possible, one builds two boxes around the target (see figure 1). The inner box is a surface from which a near field to far field transformation is applied. The outer box has perfectly matched absorber boundary conditions applied to its surfaces. Both boxes can be very near to the target, typically less than a wavelength away. An excellent commercial code (HFSS*) is available and was used for the FE calculations presented here. This code has an adaptive meshing capability to help speed convergence.

Several interesting RCS targets—a propeller, a trihedron, some very thin plates, and a metal cylinder—were analyzed in this effort. The targets were drawn in SolidWorks[†] 2007, meshed for MOM code analysis using Hypermesh,[‡] or imported into HFSS as STEP 203 files. With one exception, the calculations were run on a Dell 7400 Linux 2.8 GHz workstation with two quad-core processors, each with 1 GB of RAM. Run times were typically a few minutes to a few hours.

RCS data for the propeller at 10, 15, and 34 GHz were also obtained in a small indoor test facility at the U.S. Army Research Laboratory (ARL).

¹Gibson, W. C. *The Method of Moments in Electromagnetics*; Chapman and Hall/CRC, Taylor and Francis Group: Boca Raton, FL.

²FEKO, distributed by EM Software and Systems (USA), Inc., Hampton, VA.

³CST Microwave Studio, CST of America, Inc., U.S. Headquarters: Framingham, MA.

*HFSS is a registered trademark of ANSYS, Inc., Canonsburg, PA.

[†]SolidWorks is a registered trademark of the SolidWorks Corporation, Concord, MA.

[‡]Hypermesh is a registered trademark of Altair Engineering, Troy, MI.

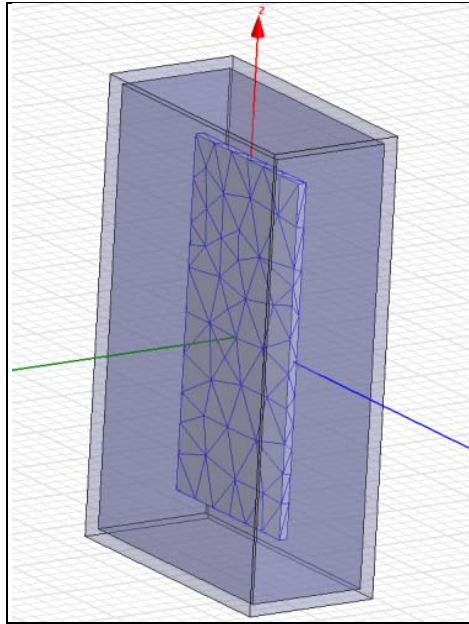


Figure 1. A metal plate meshed for FE analysis with the near-to-far field box (darker) and the perfectly matched layer box lighter also shown.

2. Results

Figure 2 shows a model propeller for a small unmanned aerial vehicle (UAV) suitable for RCS modeling and a small UAV propeller that is actually used. The initial grid for HFSS RCS analysis at 3 GHz is also shown. We were unable to mesh the real propeller in a manner suitable for analysis by either code, probably because it is so thin (the average thickness is >0.005 in) and very curved. The model propeller is about 5 in long and 0.1 in thick. The propeller is in the vertical position, the elevation angle is 0° (i.e., we are looking head-on), and the azimuthal angle was swept from 0° to 180° in all analyses.

At 3-GHz, the propeller is basically a small antenna that is primarily responsive to vertical transmit, vertical receive (VV) signals, as shown in figure 3. The dark-blue curve is the VV RCS from the MOM code, which is typically less than a dB lower than that predicted by HFSS (light-blue curve). The horizontal transmit, horizontal receive (HH) RCS calculated using the MOM code is shown as the dark-green curve, which is about 1 dB lower than the RCS predicted by HFSS shown as the light-green curve. The target was treated as a perfect electrical conductor in the analyses. It would be hard to measure these differences even in a very good compact range.

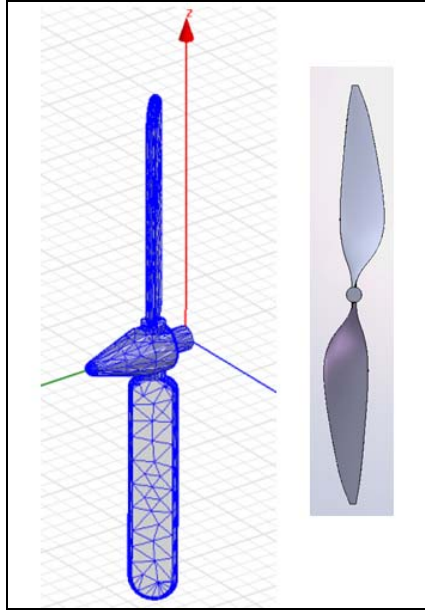
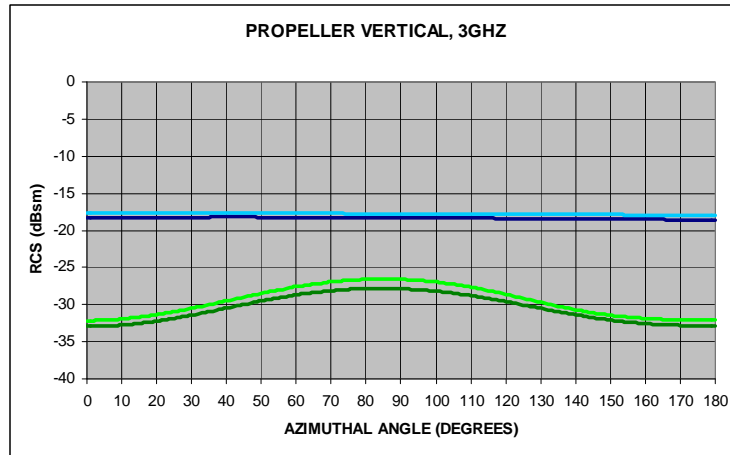


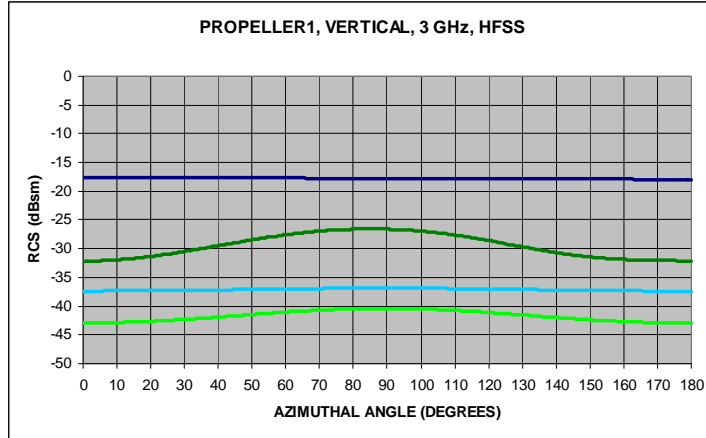
Figure 2. The model propeller used in the analyses (left) and a real propeller for a small UAV (right).



Notes: dark blue = VV-POL (MOM code), light blue = VV-POL (HFSS), dark green = HH-POL (MOM code), and light green = HH-POL (HFSS).

Figure 3. The calculated 3-GHz RCS at a 0° elevation angle of the model propeller.

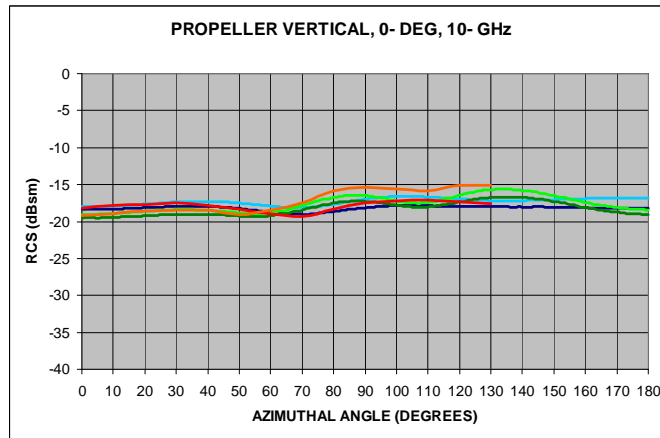
Most small UAV propellers would be made of plastic to minimize weight. One very convenient feature of the HFSS code is that it can handle dielectric materials as easily as it can handle metals. Figure 4 shows how the 3-GHz RCS of the model propeller decreases when its material is changed from metal (dark curves) to an insulating material with a dielectric constant of 3.5. The VV RCS drops by 20 dB and the HH RCS drops by 10–15 dB, depending on the azimuthal angle.



Notes: Plastic propeller: light blue = VV-POL, light green = HH-POL.
 Metal propeller: dark blue = VV-POL, dark green = HH-POL.

Figure 4. The 3-GHz RCS at a 0° elevation angle of the model propeller calculated using HFSS.

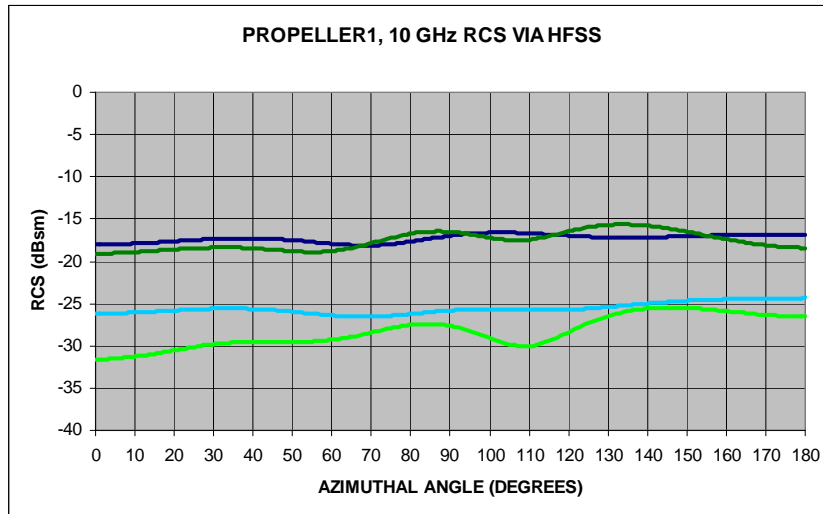
At 10 GHz, the VV and HH RCS of the metal propeller are pretty much the same, as shown in figure 5. The MOM code and HFSS results are within about 1.5 dB of each other. The VV experimental data also agrees with both predictions within 1.5 dB. The HH data differs from the predictions by >2.5 dB.



Notes: Dark blue = VV-POL (MOM code), light blue = VV-POL (HFSS), dark green = HH-POL (MOM code), light green = HH-POL (HFSS), red = VV-POL measured, and orange = HH-POL, measured.

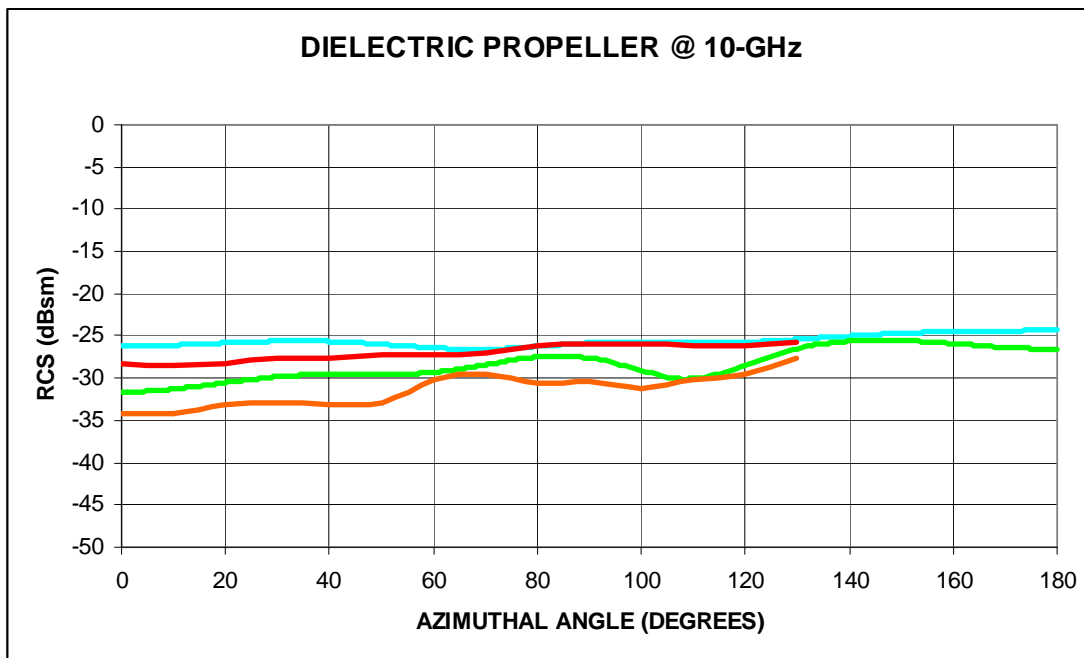
Figure 5. The 10-GHz RCS at a 0° elevation angle of the metal propeller.

Figure 6 shows the 10-GHz RCS of the metal and dielectric propellers calculated using HFSS. The VV RCS of the dielectric propeller is a little >10 dB below the metal propeller, and the HH RCS is about 12 dB lower. Figure 7 shows the calculated and measured RCS for the dielectric propeller. The measured VV RCS agrees with the calculated value to within 3 dB or better, and the HH RCS agrees with in 5 dB or better.



Notes: Plastic propeller: light blue = VV-POL, light green = HH-POL. Metal propeller: dark blue = VV-POL, dark green = HH-POL.

Figure 6. The 10-GHz RCS at a 0° elevation angle of the model propeller calculated using HFSS.



Notes: Light blue = VV-POL (HFSS), light green = HH-POL (HFSS), red = VV-POL measured, and orange = HH-POL, measured.

Figure 7. The 10-GHz RCS at a 0° elevation angle of the dielectric propeller.

Figure 8 shows the test arrangement for X and Ku bands (8–12 and 12–18 GHz), and figure 9 shows a diagram of the Ka (26.5–40 GHz) band test arrangement. The target-to-horn distance was 17 ft for the lower frequencies and 12 ft for Ka band. The measurements were bistatic in both cases, with a bistatic angle of 3.2° . Data presented are the average RCS taken at 401 frequency points in the 8–18 and 26.5–40 GHz bands using an Agilent Technologies 8510 vector network analyzer at 5° azimuthal angle increments. The noise floor in the range (without the target) was below -45 dBsm in all cases. The possibility of a multibounce interaction between the mount and the propeller can not be discounted, although none was evident on visual inspection. Mounting the propeller so that it was exactly vertical proved to be very difficult, and may not have been completely successful. Any effects of multibounce interactions or improper alignment would be more evident the higher the frequencies. Figure 10 shows a close-up view of the propeller mounted for test. Both a metal propeller and a nylon propeller were tested. These targets were fabricated in the ARL machine shop. The azimuthal angle sweep was limited to 130° to avoid exposing the rear of the mounting post. Our experience at ARL is that the 3.2° bistatic angle data is almost no different from normal incidence monostatic data.

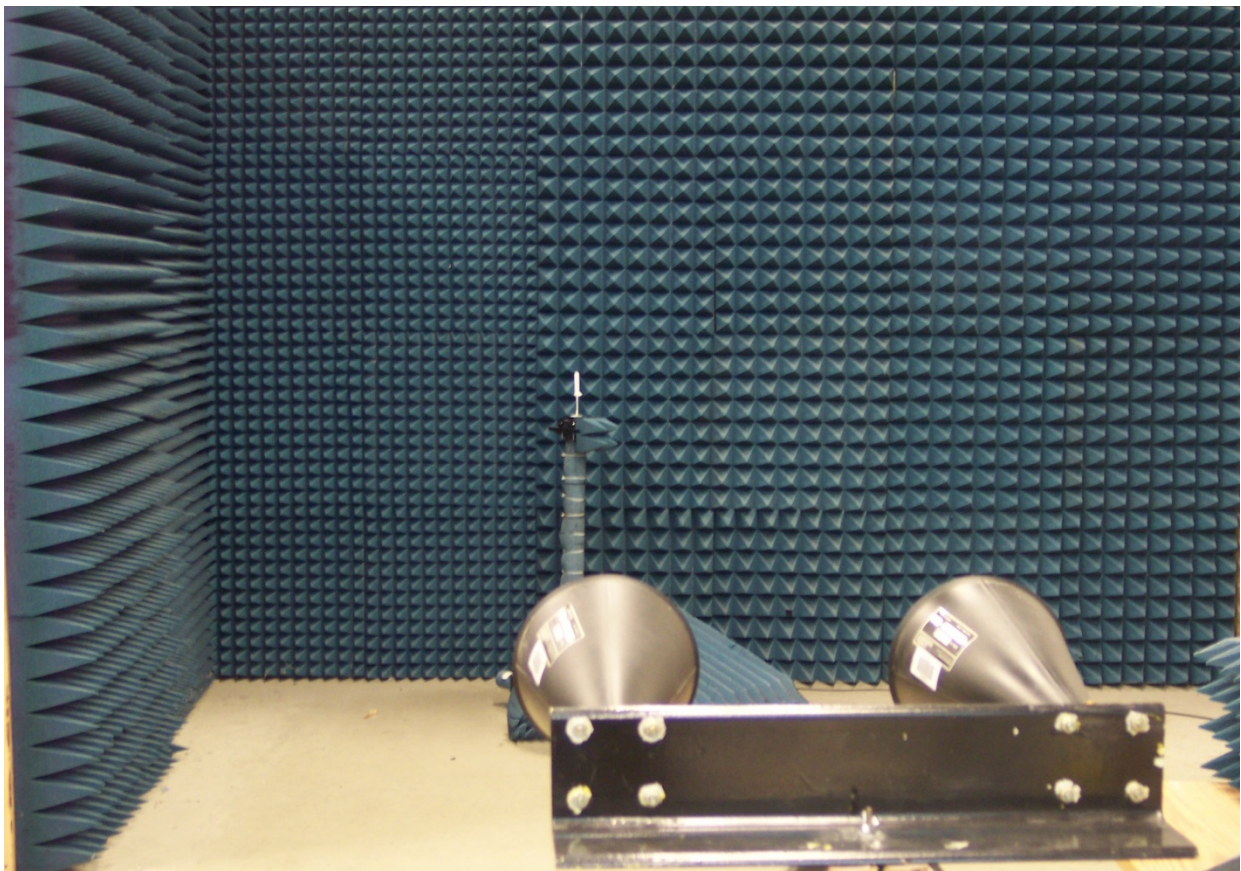


Figure 8. The test arrangement for 8–18 GHz RCS tests.

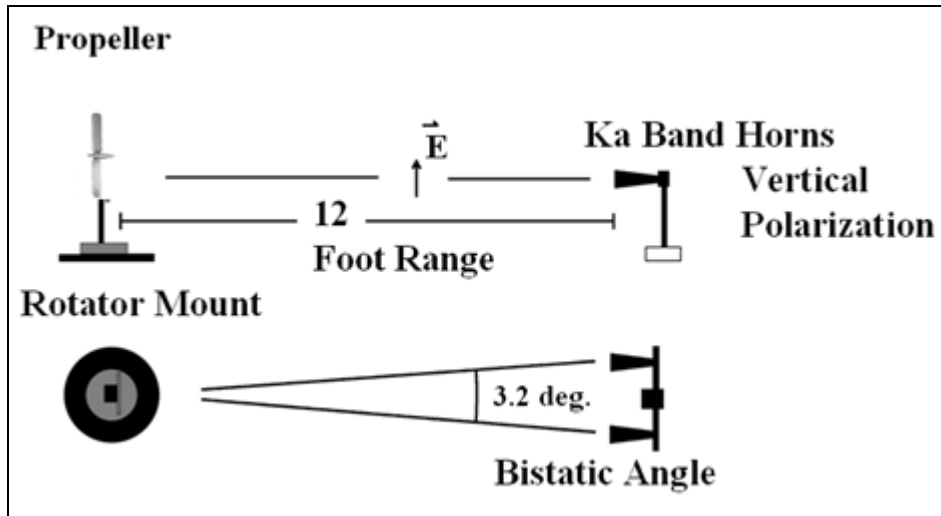


Figure 9. A diagram of the Ka band test arrangement for VV polarization.

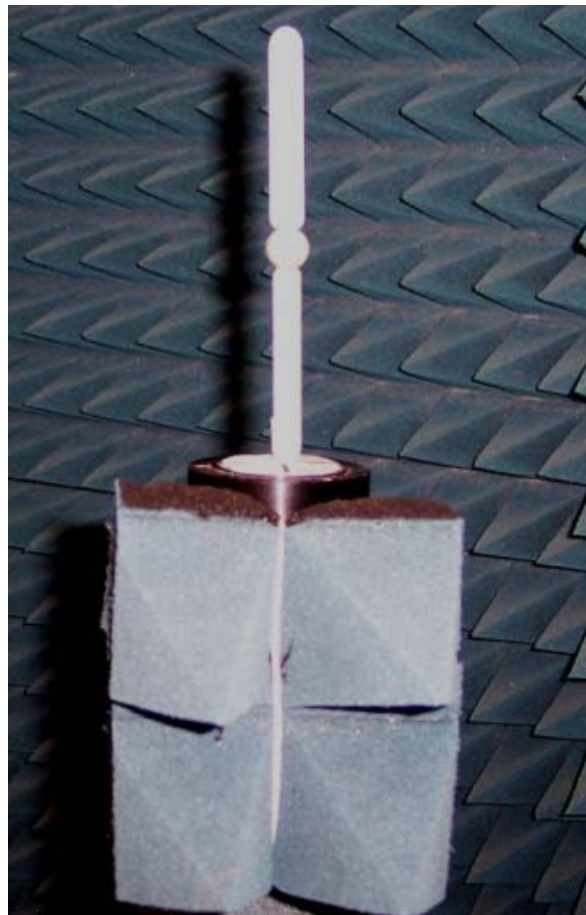
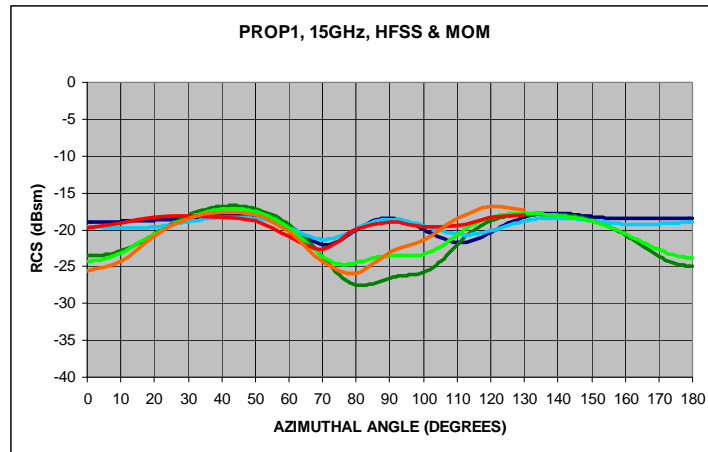


Figure 10. A close-up view of the propeller mounted for testing.

In view of the difficulties in the tests and the extended frequency range for the data set, the agreement between the data and the calculations is quite good at 10 GHz. It is also not surprising that the data for the metal propeller agrees with experiment better than for the plastic propeller.

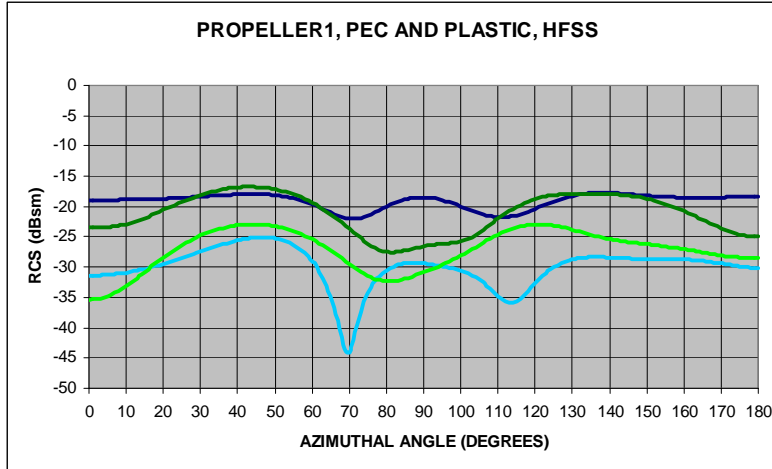
Figure 11 shows the results for the metal propeller at 15 GHz. The VV results agree very well (within about 1 dB) except at the largest azimuthal angles, where the measured data are a few decibels higher. The HH results calculated with the two codes differ by up to 3 dB between 75° and 110° azimuth but are in much better agreement over the rest of the 0°–180° range. The HH data are within 1.5 dB of either of the calculated results between 0° and 75° azimuth. They differ from the results calculated with the MOM code by as much as 5 dB and with the HFSS results by as much as 3 dB between 75° and 130° azimuth.



Notes: Dark blue = VV-POL (MOM code), light blue = VV-POL (HFSS), dark green = HH-POL (MOM code), light green = HH-POL (HFSS), red = VV-POL measured, and orange = HH-POL, measured.

Figure 11. The 15-GHz RCS at a 0° elevation angle of the metal propeller.

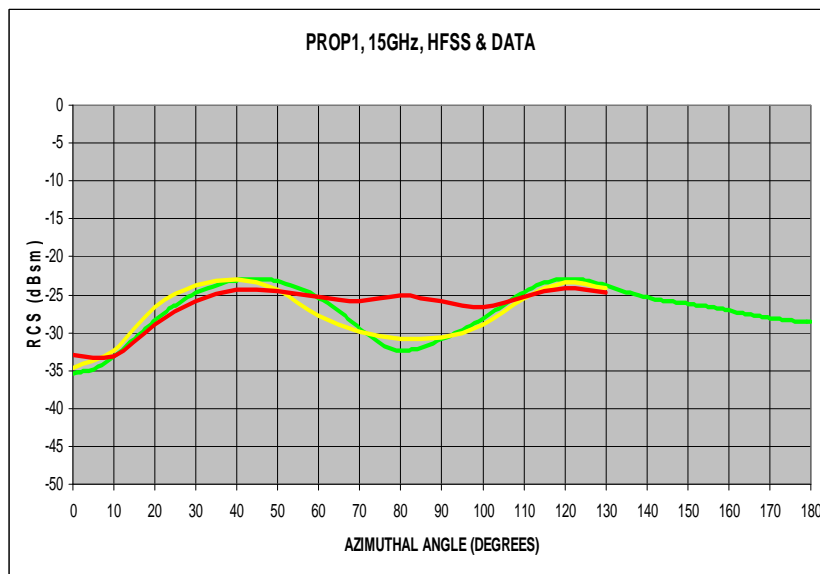
Figure 12 shows the 15-GHz RCS at a 0° elevation angle for the metal and plastic propeller calculated using HFSS. Note that the VV RCS is now generally lower than the HH RCS for the plastic propeller. The VV RCS for the plastic propeller is also generally about 10 dB lower than the VV RCS for the metal propeller. The HH RCS of the plastic propeller is generally about 5 dB lower than that of the metal, although it does come within 2–3 dB of that of the metal between about 100° and 115° azimuth.



Notes: Plastic propeller: light blue = VV-POL, light green = HH-POL. Metal propeller: dark blue = VV-POL, dark green = HH-POL.

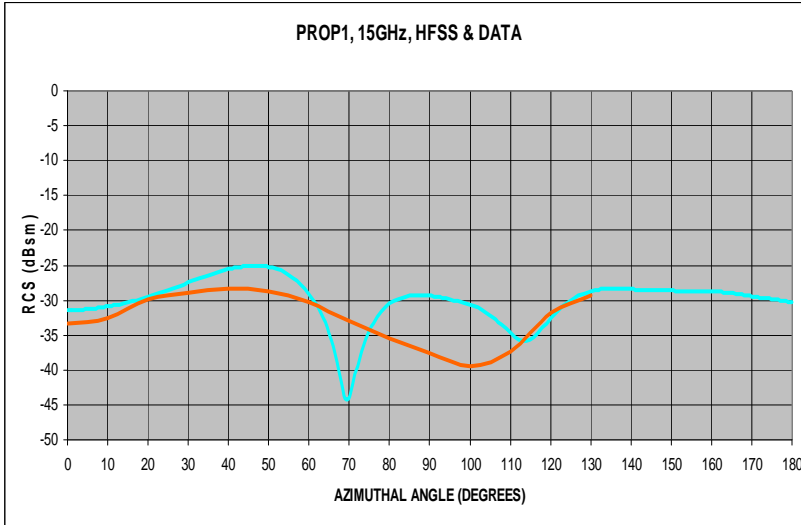
Figure 12. The 15-GHz RCS at a 0° elevation angle of the model propeller calculated using HFSS.

The calculated HH RCS for the plastic propeller is also shown in figure 13 (light-green curve) along with the best of two measurements taken after repositioning the target. The average of the two sets of measurements is also shown. The VV measurements, shown in figure 14, did not turn out as well for reasons that are not clear. The RCS between 60° and 115° azimuth, where the difference in measured and calculated is greatest, is quite low. Errors in either measured or calculated results are most likely to occur here. The sensitivity of the RCS of the propeller to positioning increases with frequency.



Notes: Light green = HFSS calculation, yellow = best of two measurements, and red = average of 2 measurements.

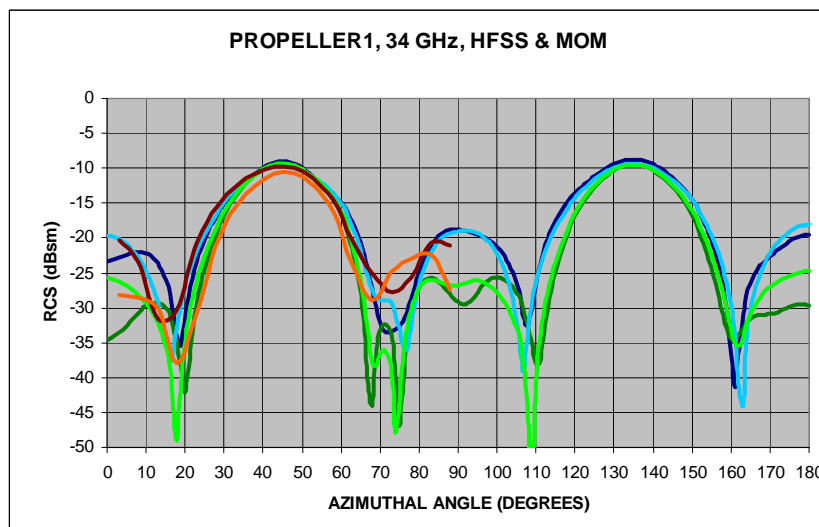
Figure 13. The 15-GHz HH RCS for the plastic propeller.



Notes: Light blue = HFSS and orange = averaged data of two experiments.

Figure 14. The 15-GHz VV RCS for the plastic propeller.

The 34-GHz RCS for the metal propeller is shown in figure 15. Results at this frequency are very sensitive to the alignment of the propeller. The main peaks at 45° and 135° in both codes agree well with each other. However, the minima are at slightly (1° to 2°) different azimuthal angles. It is possible that the alignment of the propeller is slightly different for the two codes, but this seems unlikely, and there is no way to check this out. The differences between the VV and HH polarizations predicted by the two codes are in good agreement where the RCS is above -20 dBsm. The measured data is very sensitive to the alignment of the propeller, but the agreement where the RCS is above -20 dBsm is reasonably good.

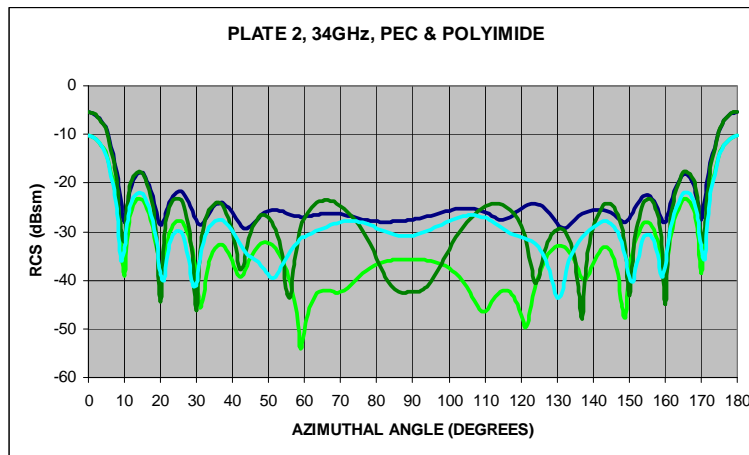


Notes: Dark blue = VV-POL (MOM code), light blue = VV-POL (HFSS), dark green = HH-POL (MOM code), light green = HH-POL (HFSS), red = VV-POL measured, and orange = HH-POL, measured.

Figure 15. The 34-GHz RCS at a 0° elevation angle of the metal propeller.

A 2-in-high, 1-in-wide plate (see figure 1) was also analyzed to develop an understanding of how the RCS of the propeller will depend on thickness and material at 34 GHz. Thicknesses of 100, 50, 10, and 5 mil were explored, both metallic perfect electric conductor or PEC and polyimide with a dielectric constant of 3.5. The calculations were run using HFSS.

For a 100-mil thickness, figure 16, the dielectric plate is about a half wavelength thick at normal incidence. The RCS of the dielectric plate is 3 to 4 dB lower than that of the metal plate out to about 15° azimuth. Between 15° and 90° azimuth, the VV and HH RCS for the metal plate differ by as much as 15 dB, the HH RCS generally being lower. The RCS of the dielectric plate is even lower, as shown in figure 16.

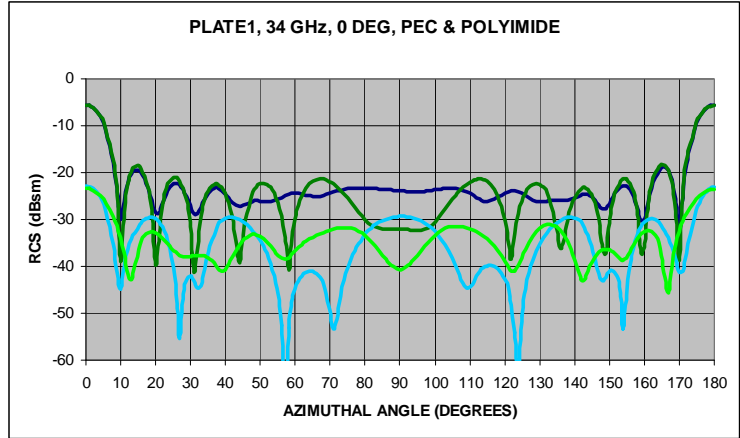


Notes: Dark blue = VV metal, light blue = VV dielectric, dark green = HH metal, and light green = HH dielectric.

Figure 16. The calculated RCS of the 100-mil-thick 1- × 2-in plate at 34 GHz.

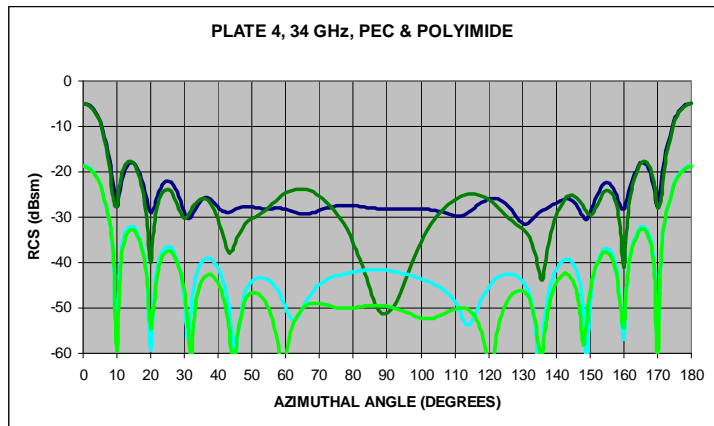
The 50-mil-thick dielectric plate is about a quarter of a wavelength thick at 34 GHz. The RCS of the dielectric plate at normal incidence is ~15 dB lower than the metal plate and never rises above -23 dBsm. In fact, it is below -30 dBsm over much of the angular range. The calculated results for the 50-mil-thick plate are shown in figure 17.

A real propeller for a small UAV would likely be much thinner than these plates, typically in the 5–10-mil range. The calculated RCS for 10-mil-thick metal and dielectric plates is shown in figure 18. The RCS of the dielectric plate has a maximum of about -18 dBsm at normal incidence, and is below -30 dBsm for angles between 8° and 172°. The VV and HH RCS for the dielectric plate track each other more closely than for thicker targets.



Notes: Dark blue = VV metal, light blue = VV dielectric, dark green = HH metal, and light green = HH dielectric.

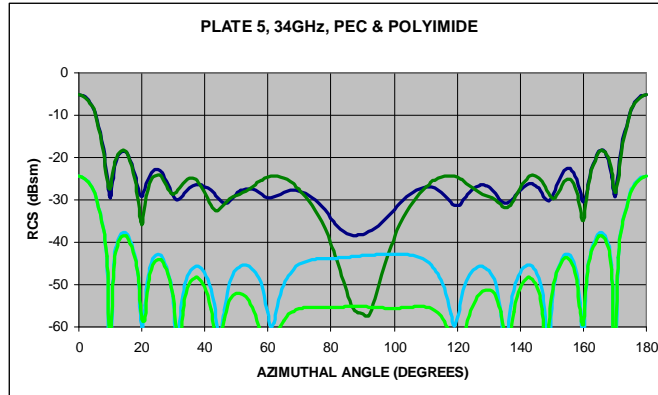
Figure 17. The calculated RCS of the 50-mil-thick 1- × 2-in plate at 34 GHz.



Notes: Dark blue = VV metal, light blue = VV dielectric, dark green = HH metal, and light green = HH dielectric.

Figure 18. The calculated RCS of the 10-mil-thick 1- × 2-in plate at 34 GHz.

The RCS plots for 5-mil-thick metal and dielectric plates are shown in figure 19. The Maximum RCS of the dielectric plate is about -24 dBsm near normal incidence. The RCS falls off rapidly as the target is moved away from normal incidence and is generally below -40 dBsm. The RCS of the metal plate is typically ~20 dB higher. A 5-mil-thick dielectric propeller would be very difficult to detect unless the radar was looking right at a flat surface if the propeller has one.



Notes: Dark blue = VV metal, light blue = VV dielectric, dark green = HH metal, and light green = HH dielectric.

Figure 19. The calculated RCS of the 5-mil-thick 1- × 2-in plate at 34 GHz.

A second target of interest is the trihedron shown in figure 20. This target has a base 24-in square, and 1-in-high sides. The base and sides are 0.375 in thick. In previous calculations at 10-GHz, this target had shown an unusual RCS pattern at small elevation angles. The VV component was large and the HH component was highly suppressed so that it was well below the cross-polarized RCS components. This target was a little to large to run at 10 GHz in HFSS with the available RAM, so it was run at 5 GHz instead.

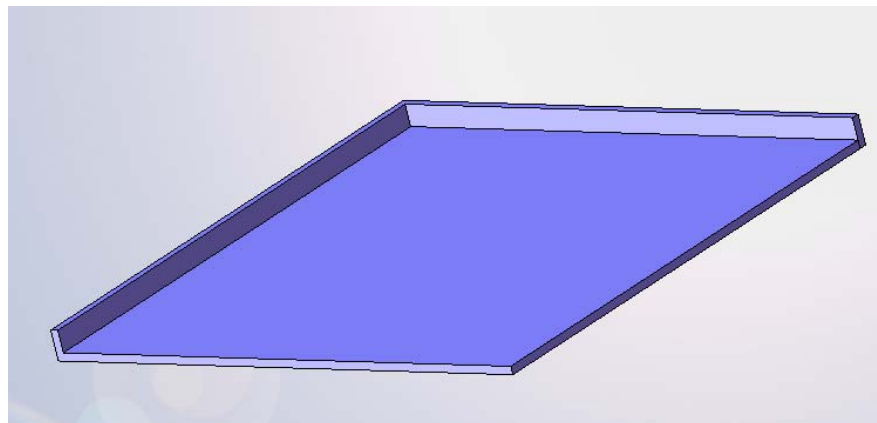
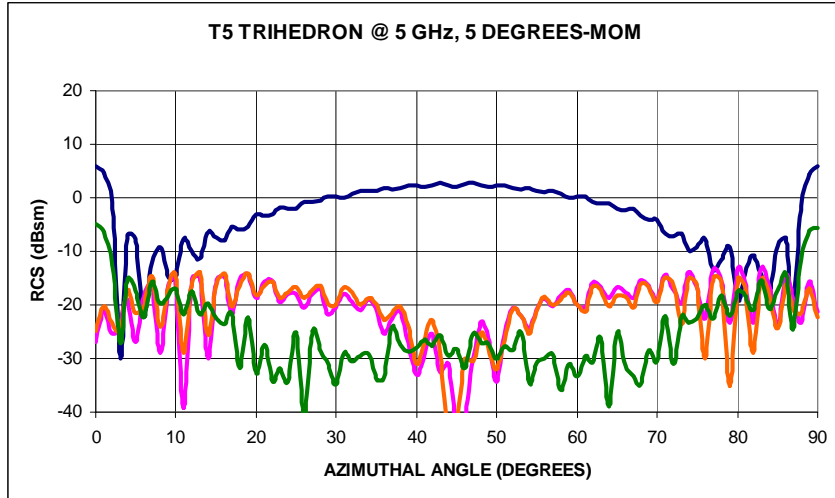


Figure 20. The trihedron analyzed in this study.

The RCS of the trihedron depends strongly on the elevation angle. The RCS at a 5° elevation angle calculated using the MOM code is shown in figure 21. The maximum VV RCS is about 30 dB higher than the HH RCS at a 45° azimuthal angle.



Notes: Dark blue = VV POL, dark green = HH POL, red = VH POL, and orange = HV POL.

Figure 21. The 5-GHz RCS at a 5° elevation angle calculated using a MOM code.

The VV component of the RCS is by far the most important since it is the largest. Figure 22 compares this component calculated using the MOM code and HFSS. The agreement is within about 1 dB over most of the angular range. Significant differences occur only at angles at which there is a deep null at which the actual value of the RCS is not particularly important.

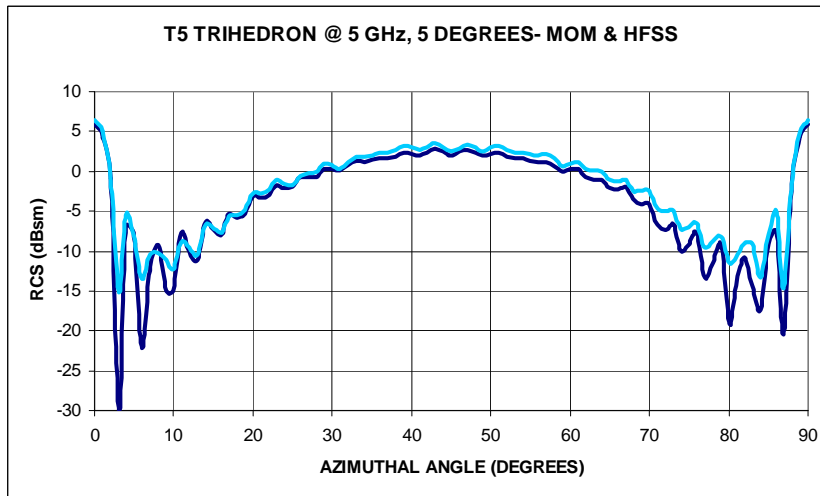


Figure 22. The 5-GHz VV RCS at a 5° elevation angle calculated using the MOM code (dark blue) and HFSS (light blue).

Figure 23 shows the rest of the RCS. The HH POL RCS (light-green curve) calculated using HFSS agrees very well with the MOM code results (dark-green curve) from about 0° to 3° and 87° to 90° azimuth. However, it converges more nearly to the VH RCS at the other azimuthal angles.

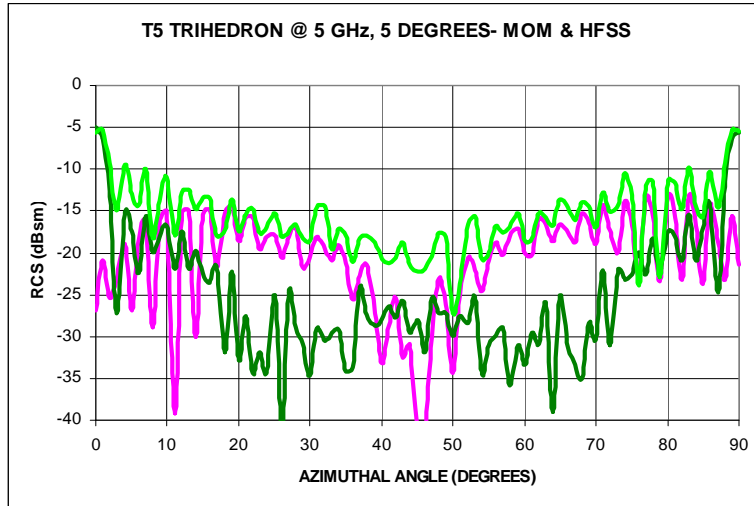
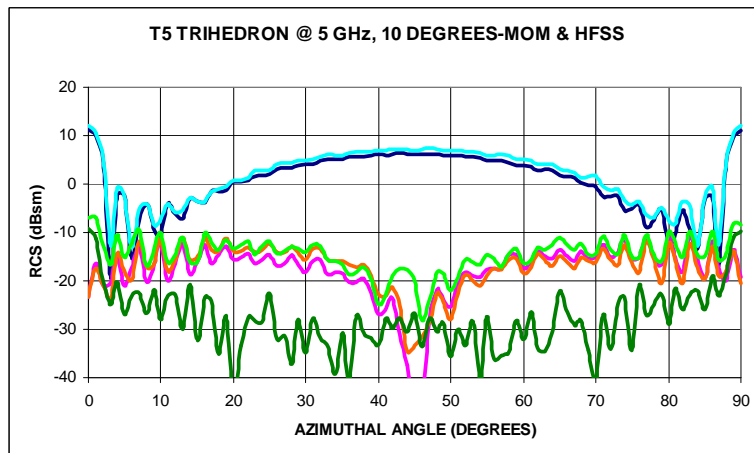


Figure 23. The HH polarized 5-GHz RCS at a 5° elevation angle calculated using HFSS (light-green curve) and the MOM code (dark-green curve). The red curve is the VH RCS calculated using the MOM code.

The computed results at a 10° elevation angle (figure 24) exhibited the same characteristics. The VV results computed using the two codes agreed very well, even better than at a 5° elevation angle. The HH results in HFSS still converged to the VH results calculated using the MOM code, however.



Notes: Dark blue = VV POL (MOM), light blue = VV POL (HFSS), dark green = HH POL (MOM), light green = HH POL (HFSS), red = VH POL (MOM), and orange = HV POL (MOM).

Figure 24. The RCS at a 10° elevation angle calculated using a MOM code and HFSS.

In order to try to get the HFSS and MOM code HH results to agree better, the problem was run using HFSS on a computer with much more memory and the convergence criterion was tightened so that the RCS difference between passes was less than 0.5 dB. The problem took a lot more memory (29 GB) and time (9 h), but the results, shown in figure 25, agree very well with the MOM code results. This is impressive since the HH RCS is very low, generally in the 30-dBsm range. The HFSS results are about 2 dB higher near 0° and 90°, however.

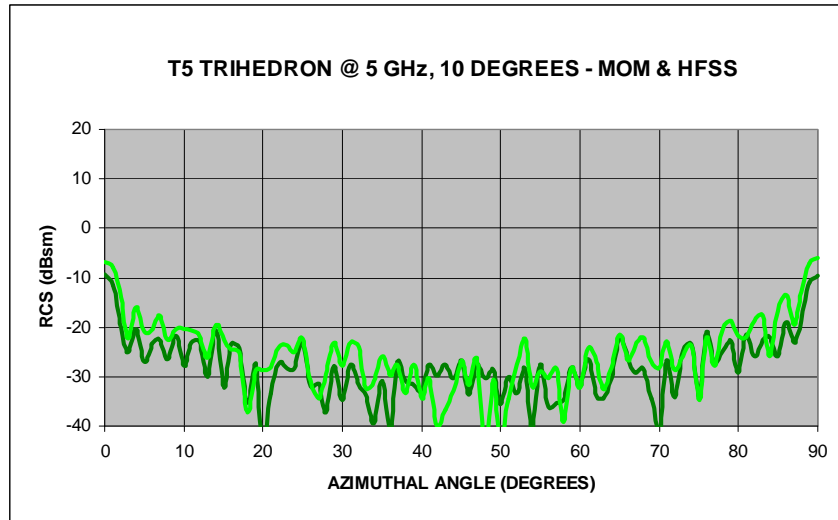
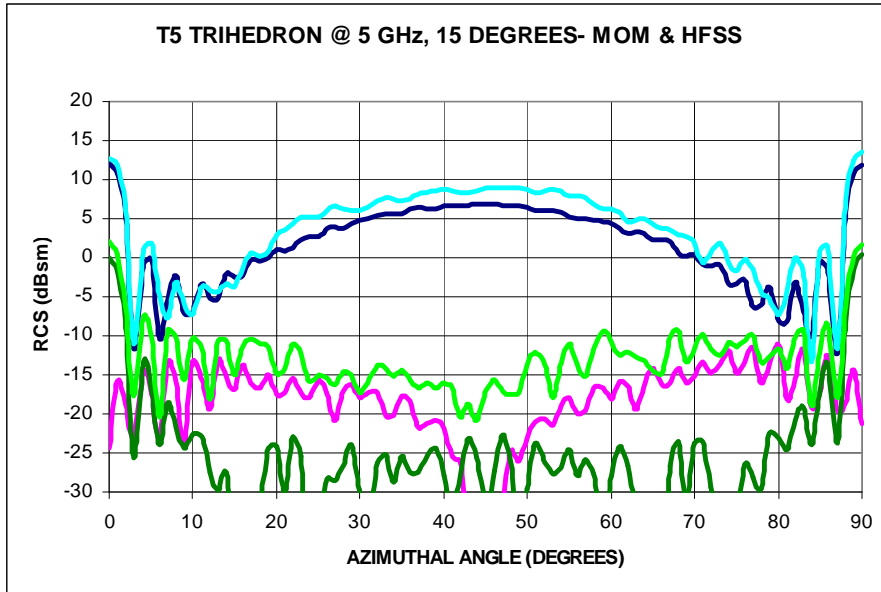


Figure 25. The HH RCS for the trihedron at a 10° elevation angle calculated using the MOM code (dark green) and using HFSS with increased accuracy (light green).

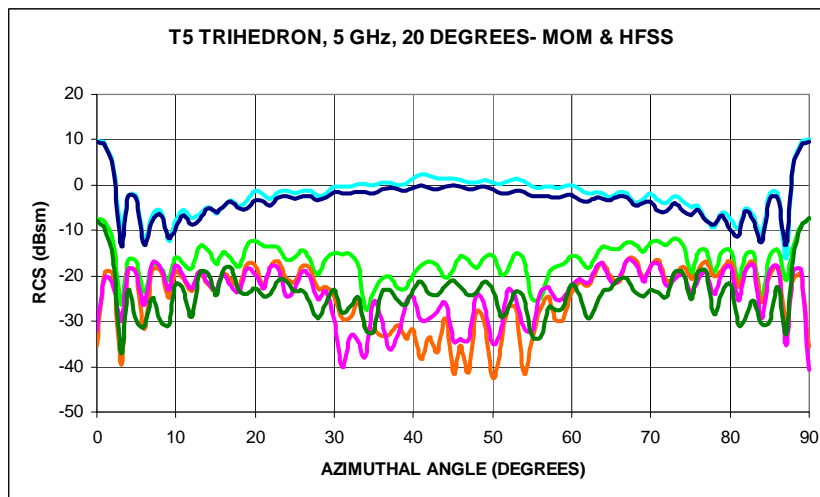
Figure 26 shows the calculated 5-GHz RCS at a 15° elevation angle using the 8-GB RAM computer. The VV RCS calculated using HFSS (light blue curve) is about 2 dB higher than that calculated using the MOM code (dark blue curve). The HH RCS calculated using HFSS again converges more nearly to the VH/HV RCS calculated using the MOM code over most of the angular range. The agreement with the HH RCS calculated using the MOM code is very good in the regions where it is significant, from 0° to 3° and 87° to 90° azimuth.

The 5-GHz RCS at a 20° elevation angle is shown in figure 27. The VV RCS calculated using the two codes are in excellent agreement, generally better than 1 dB. The HH RCS near the end points of the sweep are also in good agreement where the HH RCS is in the -10 dBsm range. The VH/HV and HH RCS calculated using the MOM code is generally below -20 dBsm. The HH RCS calculated using HFSS is 0-5 dB higher, however. This is still quite low and not very important. The agreement could almost certainly be improved upon by using a different convergence criterion and more RAM, as was done for the 10° elevation case.



Notes: Dark blue = VV POL (MOM), light blue = VV POL (HFSS), dark green = HH POL (MOM), light green = HH POL (HFSS), and red = VH POL (MOM).

Figure 26. The 5-GHz RCS at a 15° elevation angle calculated using a MOM code and HFSS.



Notes: Dark blue = VV POL (MOM), light blue = VV POL (HFSS), dark green = HH POL (MOM), light green = HH POL (HFSS), red = VH POL (MOM), and orange = HV POL (MOM).

Figure 27. The 5-GHz RCS at a 20° elevation angle calculated using a MOM code and HFSS.

On the whole, the agreement between the two codes was quite acceptable in regions where the RCS was significant. In view of the differences in computational methods, this is very satisfying.

One other target was briefly examined. This was a 1-in-diameter, 4-in-long, right-circular cylinder viewed end-on (figure 28). The VV RCS was calculated for 401 frequencies between 26.5 and 40 GHz. The results from the two codes are plotted in figure 29. The agreement is very good considering that no unusually tight convergence criteria were applied in either code.

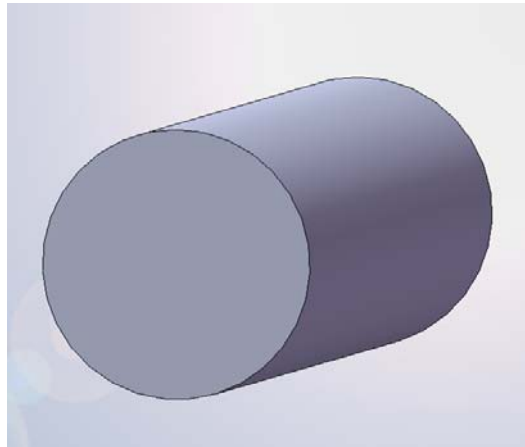


Figure 28. The 1-in-diameter, 4-in-long cylinder analyzed.

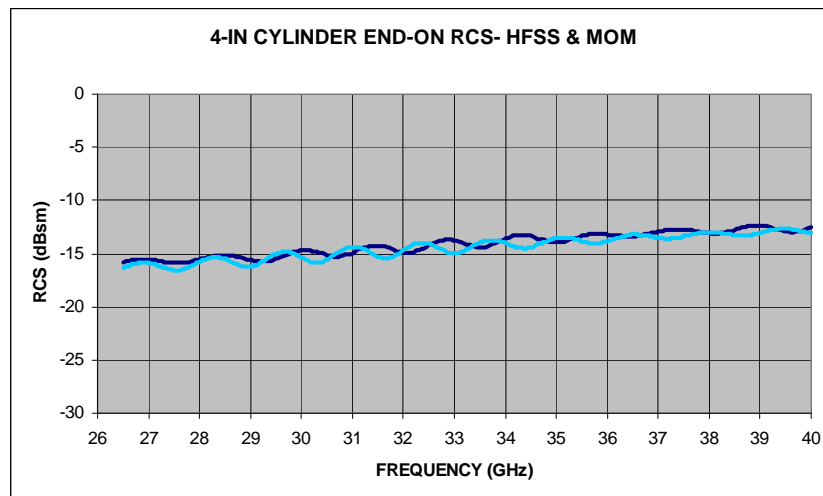


Figure 29. The end-on VV RCS of the cylinder calculated using a MOM code (light blue) and HFSS (dark blue).

3. Conclusions

We have compared RCS results calculated using a MOM code and HFSS, an FE code. The agreement between the two sets of results has generally been within a few decibels where the RCS was large enough to matter. Since default meshing and default convergence parameters were used for most of the HFSS calculations, the quality of the agreement must be regarded as satisfactory. For the one case where the default parameters were not adequate, the RCS was sufficiently low enough to not be of concern. Changing the convergence parameters brought the predictions of the two codes into excellent agreement.

FE codes are necessarily much more RAM intensive than MOM codes, but RAM for workstations has become much less expensive than in the past. The FE code also easily adapts to dielectric materials, which is a very desirable feature.

NO. OF
COPIES ORGANIZATION

1 DEFENSE TECHNICAL
(PDF INFORMATION CTR
only) DTIC OCA
8725 JOHN J KINGMAN RD
STE 0944
FORT BELVOIR VA 22060-6218

1 DIRECTOR
US ARMY RESEARCH LAB
IMNE ALC HRR
2800 POWDER MILL RD
ADELPHI MD 20783-1197

1 DIRECTOR
US ARMY RESEARCH LAB
RDRL CIM L
2800 POWDER MILL RD
ADELPHI MD 20783-1197

1 DIRECTOR
US ARMY RESEARCH LAB
RDRL CIM P
2800 POWDER MILL RD
ADELPHI MD 20783-1197

1 DIRECTOR
US ARMY RESEARCH LAB
RDRL D
2800 POWDER MILL RD
ADELPHI MD 20783-1197

ABERDEEN PROVING GROUND

1 DIR USARL
RDRL CIM G (BLDG 4600)

NO. OF
COPIES ORGANIZATION

1 HQ DA
DAMI FIT
NOLAN BLDG
WASHINGTON DC 20310-1025

2 DIRECTOR
US ARMY NGIC
IANG RSG
W NIXON
J SIZEMORE
2055 BOULDERS RD
CHARLOTTESVILLE VA
22091-5391

1 COMMANDER
USAMC
AMXMI INT
9301 CHAPEK RD
FT BELVOIR VA 22060-5527

1 COMMANDER
USA ARMAMENT RD&E
SMCAR AS CTR
PICATINNY ARSENAL NJ
07806-5000

1 US ARMY RSRCH OFC
J PRATER
PO BOX 12211
RSRCH TRIANGLE PARK NC
27709-2211

1 UDLP
R BRYNSVOLD
4800 E RIVER RD
MINNEAPOLIS MN 55421-1498

1 DIRECTOR
NGIC
IANG TMT
2055 BOULDERS RD
CHARLOTTESVILLE VA
22091-5391

6 DIR USARL
RDRL SER U
C LE
W COBURN
C KENYON
A SULLIVAN
T DOGARU
J SICHNA
2800 POWDER MILL RD
ADELPHI MD 20783-1197

NO. OF
COPIES ORGANIZATION

3 COMMANDER
US ARMY TACOM
AMSRD TAR R
C KOLP
T GONDA
H MOLITORIS
WARREN MI 48397-5000

1 GDLS
M PASIK
PO BOX 1800
STERLING HEIGHTS MD 48090-1800

1 MMW CONCEPTS LLC
HDG CORP CTR
H B WALLACE
224 N WASHINGTON ST
HAVRE DE GRACE MD 21078

1 GENERAL DYNAMICS LAND
MAIL ZONE 435 01 24
K KAO
38500 MOUND RD
STERLING HEIGHTS MI
48310-3200

1 GENERAL DYNAMICS LAND
MAIL ZONE 437 02 00
S HALL
38500 MOUND RD
STERLING HEIGHTS MI
48310-3200

4 US ARMY AVN & MISSILE CMND
AMSRD AMR AS CC
J BAEDER
BLDG 5400
FOWLER RD B 354
REDSTONE ARSENAL AL 35898

1 US ARMY AVN & MISSILE CMND
AMSRD AMR AS PT
J MCNUTT
BLDG 5464
FOWLER RD
REDSTONE ARSENAL AL 35898

1 US ARMY AVN & MISSILE CMND
AMSRD AMR SS
R KRETZSCHMAR
BLDG 5400
FOWLER RD E-338
REDSTONE ARSENAL AL 35898

NO. OF
COPIES ORGANIZATION

NO. OF
COPIES ORGANIZATION

1 US ARMY AVN & MISSILE CMND
AMSRD AMR WD SG SD
B NOURSE
BLDG 5400
FOWLER RD A 268
REDSTONE ARSENAL AL 35898

RDRL WMM E
M BRATCHER
T JESSEN
P DEHMER
RDRL WMP
P BAKER
RDRL VT
S WILKERSON

2 ANSOFT CORP
N HIRTH
K FERREIRA
25 BURLINGTON MALL RD 5TH FL
BURLINGTON MA 01803

ABERDEEN PROVING GROUND

1 DIRECTOR
USAMSA
AMSRD AMS TD
K WEYGANT
392 HOPKINS RD
APG MD 21005-5071

25 DIR USARL
RDRL CI
R NAMBURU
RDRL CIH C
E MARK
RDRL SL
R COATES
RDRL SLB W
K FROUNFELKER
RDRL WM
P PLOSTINS
RDRL WML F
D LYON
J CONDON
G KATULKA
R MCGEE
RDRL WMM
J ZABINSKI
RDRL WMM A
R BOSSOLI
S CORNELISON
M MAHER
W SPURGEON (3 CPS)
RDRL WMM B
M VANLANDINGHAM
RDRL WMM C
K CHESONIS
RDRL WMM D
E CHIN